Nanoscale

PAPER

View Article Online
View Journal | View Issue

Check for updates

Cite this: *Nanoscale*, 2024, **16**, 2419

Few-layered graphene increases the response of nociceptive neurons to irritant stimuli†

Lieselot Deleye,‡[a] Francesca Franchi,‡[a,b] Martina Trevisani,[a,c] Fabrizio Loiacono,[b] Silvia Vercellino,[a,b] Doriana Debellis,[d] Nara Liessi,[e] Andrea Armirotti,[e] Ester Vázquez,[f] Pierluigi Valente,*§[b,c] Valentina Castagnola*§[a,b] and Fabio Benfenati*§[a,b]

The unique properties of few-layered graphene (FLG) make it interesting for a variety of applications, including biomedical applications, such as tissue engineering and drug delivery. Although different studies focus on applications in the central nervous system, its interaction with the peripheral nervous system has been so far overlooked. Here, we investigated the effects of exposure to colloidal dispersions of FLG on the sensory neurons of the rat dorsal root ganglia (DRG). We found that the FLG flakes were actively internalized by sensory neurons, accumulated in large intracellular vesicles, and possibly degraded over time, without major toxicological concerns, as neuronal viability, morphology, protein content, and basic electrical properties of DRG neurons were preserved. Interestingly, in our electrophysiological investigation under noxious stimuli, we observed an increased functional response upon FLG treatment of the nociceptive subpopulation of DRG neurons in response to irritants specific for chemoreceptors TRPV1 and TRPA1. The observed effects of FLG on DRG neurons may open-up novel opportunities for applications of these materials in specific disease models.

Received 31st July 2023,
Accepted 8th January 2024

DOI: 10.1039/d3nr03790h

rsc.li/nanoscale

Open Access Article. Published on 09 Sunguti 2024. Downloaded on 2025-08-13 04:12:18.
This article is licensed under a Creative Commons Attribution-NonCommercial 3.0 Unported Licence.

Introduction

Since its discovery in 2004, remarkable efforts have been devoted to better understanding the physical and chemical properties of graphene-related materials (GRMs).[1–3] This has caused exponential growth in the applications of GRMs in a wide range of fields, from engineering to electronics to biotechnologies and biomedical applications.[2–8] GRMs are particularly interesting in neuroscience, as they could overcome the limitations of the currently used materials, such as metals and silicon, which are characterized by elevated stiffness, high inflammatory potential, and poor long-term stability under physiological conditions.[9–13] On the contrary, GRMs are characterized by a large surface area, flexibility, and excellent electrical and conductive properties.[3,9,14] They could therefore find applications as drug/gene carriers for improving imaging in the brain and as a substrate for tissue engineering.[14–22] In this view, GRMs biocompatibility with the chosen biological environment is of great importance. However, in the literature, there is controversial information about the general biocompatibility of GRMs, and it seems that their behavior might be dependent on the specific cellular model employed.[23,24] In particular, the results on neurotoxicity are contradictory as graphene has been proven to be toxic, harmless, or even beneficial to the neurons.[9,22,25–35] The type of GRM, the dose, functionalization, route of administration, and targeted cells are all factors that strongly contribute to the GRM's biological interactions.

In the central nervous system (CNS), many studies predominantly used graphene oxide (GO) or reduced GO (rGO).[36–40] There use for applications in the CNS seems promising, but their biocompatibility is still a topic for debate.[9,30,31,41–43] Instead, low concentrations of small colloidal few-layered graphene (FLG) flakes showed great biocompatibility towards hippocampal neurons, astrocytes, and blood–brain barrier (BBB).[30,31,44]

Toxicity studies of GRMs on neurons have mainly focused on the CNS.[9,30,31,45,46] Most of the information about GRMs

[a]*Center for Synaptic Neuroscience and Technology, Istituto Italiano di Tecnologia (IIT), Largo Rosanna Benzi 10, 16132 Genova, Italy.*
E-mail: valentina.castagnola@iit.it, fabio.benfenati@iit.it
[b]*IRCCS Ospedale Policlinico San Martino, Largo Rosanna Benzi 10, 16132 Genova, Italy*
[c]*Department of Experimental Medicine, Section of Physiology, University of Genova, Genoa, 16132, Italy. E-mail: pierluigi.valente@unige.it*
[d]*Electron Microscopy Facility, IIT, Via Morego 30, 16163 Genoa, Italy*
[e]*Analytical Chemistry Facility, IIT, via Morego, 30, 16163 Genoa, Italy*
[f]*Facultad de Ciencias Químicas, Universidad Castilla La-Mancha, Ciudad Real, 13071 Spain*
† Electronic supplementary information (ESI) available. See DOI: https://doi.org/10.1039/d3nr03790h
‡ Equal contribution.
§ Co-last authors.

Open Access Article. Published on 09 Sunguti 2024. Downloaded on 2025-08-13 04:12:18.
This article is licensed under a Creative Commons Attribution-NonCommercial 3.0 Unported Licence.

effects on the peripheral nervous system (PNS) refers to planar graphene-based substrates, intended as scaffolds for nerve regeneration.[19,21,47–52] Differently from the CNS, peripheral neurons and nerves lack a barrier protecting their neurons from the systemic circulation, and colloidal forms of graphene (also exfoliated from planar implants), purposely or accidentally present in the circulation, might enter in contact with the cells of the PNS. In addition, colloidal GRMs are so far scarcely investigated for their interactions with peripheral neurons.

Somatic sensory neurons, also called dorsal root ganglion (DRG) neurons, have very distinct molecular, morphological, electrical, and network properties compared to central neurons. These cells are the first-order neurons in the somatosensory afferent pathway, transducing peripheral stimuli into electrical information and conveying them to the CNS so they can be analyzed by the brain. Moreover, DRG neurons are essential regulators of pain, and pain-related disorders are known to impact human life quality significantly. GRMs might also purposely be applied to the PNS as, for instance, an analgesic drug carrier for neuropathic pain or direct neuronal regulators, and some research indeed focused on the pain-relieving effects of graphene but did not investigate its direct impact on the sensory neurons' functionality.[53,54]

In the present study, colloidal FLG was tested against primary sensory neurons to evaluate its biocompatibility using a palette of readouts, including viability, morphological changes, protein dysregulation, and electrophysiological properties. Given the polymodal nature of DRG neurons mediating diverse stimuli, in this study, we also investigated the response of these neurons to specific modalities evaluating the response to acidic pH and irritants. In this context, we tested capsaicin and allyl isothiocyanate (AITC) that selectively activate two members of the transient receptor potential (TRP) family of ion channels, TRPV1 (vanilloid) and TRPA1 (ankyrin), respectively. We found that DRG neurons, previously incubated with FLG, exhibited an increased response to both irritants, but not to mild acidic pH, a general stimulus for nociceptors. Overall, our results define the safe conditions for the use of colloidal FLG on DRG neurons and pave the way to intriguing new potential applications.

Results and discussion

Primary sensory neurons dissected from P2/P3 rat pups were used as an experimental model to assess the impact of colloidal FLG exposure. DRG cells have distinctive large, round cell bodies that protrude from the planar plane, as shown in Fig. S1A.† Under our culturing conditions, small dividing glial cells were present and necessary for the initial DRG neuron growth.[55–57] After one day *in vitro* (DIV1), the antimitotic cytosine β-D-arabinoside was added to attenuate the growth of these glial cells (Fig. S1B†). At DIV4, neurons were incubated with FLG flakes at concentrations ranging from 10 to 100 μg mL^{-1}. The characterization of our FLG is reported in our previous works.[58] One day later, we investigated FLG uptake, neuron viability, presence of apoptosis, alterations in the DRG neuron morphology, protein content, and electrical activity and characteristics.

FLG is actively internalized by DRG neurons

After DRG incubation with FLG, the presence of large flakes outside the cells was observed by optical and scanning electron microscopy (Fig. S2†). The actual internalization of FLG flakes was assessed using flow cytometry, confocal microscopy, and transmission electron microscopy (TEM).

Flow cytometry allows for quantification of graphene uptake in a well-established label-free setting,[59–61] as a function of the increased cells' granularity, which in turn increases the measured side scattering (SSC).[62] We chose not to label FLG flakes, thus avoiding any possible bias in the graphene–neuron interaction, and measured the uptake kinetics of FLG by SSC values normalized over untreated control samples (CTRL, Fig. 1A). The SSC signal for FLG-treated neurons

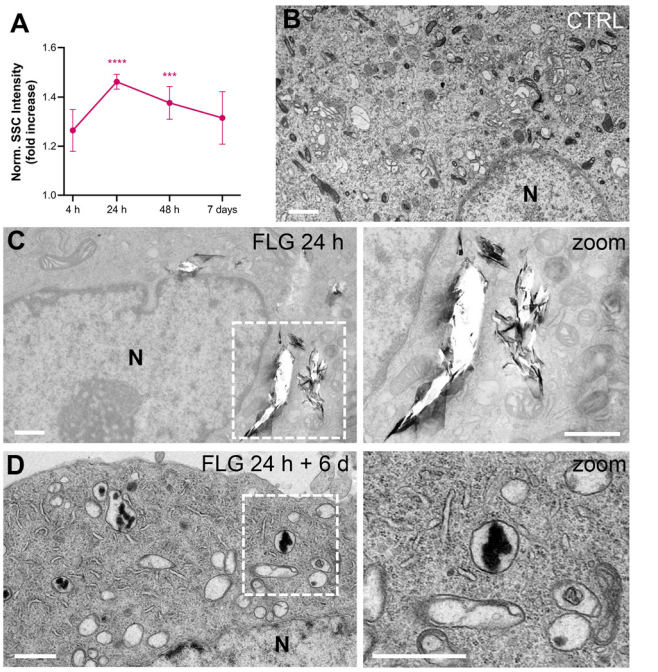

Fig. 1 Primary sensory neuron cultures, at DIV4, exposed to 10 μg mL^{-1} of colloidal FLG at different times. (A) Normalized side scatter intensity as a measure of graphene uptake over time. Data are expressed as means ± SEM, FLG: 4 h (N = 2; 2 replicates); 1 day (N = 4; 6 replicates), 2 days (N = 3; 5 replicates) and 7 days (N = 3; 5 replicates); Statistical analysis: ***p = 0.003 ****p < 0.0001 (Student's t-test *vs.* CTRL). (B–D) Representative TEM micrographs of sensory neurons (B) untreated (control), (C) exposed to FLG for 24 h, and (D) exposed to FLG for 24 h, then incubated with fresh medium and observed after further 6 days (below). The control images have a good contrast of the intracellular organelles staining, which cannot be maintained when large FLG aggregates are present in the field of view. In C, white holes in correspondence to FLG aggregates are due to the microtome slicing procedure (slice thickness, 70 nm). On the left, zoom images of vesicles containing FLG are shown for (C) and (D), showing a different FLG morphology, passing from flakes-like to amorphous carbon-like. N indicates the nuclei. Scale bars are 1 μm.

This journal is © The Royal Society of Chemistry 2024

Open Access Article. Published on 09 Sunguti 2024. Downloaded on 2025-08-13 04:12:18.
This article is licensed under a Creative Commons Attribution-NonCommercial 3.0 Unported Licence.

started increasing after 4 h incubation and reached a plateau of significant internalization after 24 h. From 48 h of incubation up to 7 days, the quantified uptake slightly decreased. This might be due to the material that, after the first 24 h, reaches a maximum of internalization, after which it becomes too aggregated in the medium to be further internalized. Also, degradation or export phenomena cannot be excluded.

Both confocal imaging and TEM were used to visualize the presence of graphene flakes inside the neurons. Graphene flakes can be visualized under a confocal microscope with mid-infrared reflective light; however, quantification through this methodology is difficult as smaller flakes might be undetectable, and some signals from the intracellular compartments might interfere.[63] From a qualitative point of view, FLG was localized intracellularly (Fig. S3†). TEM imaging confirmed this observation. In the TEM micrographs shown in Fig. 1, some FLG accumulation in intracellular vesicles is visible after 24 h of exposure (Fig. 1C) compared to untreated cells (Fig. 1B). As can be noticed from Fig. 1C, the FLG flakes appear in large aggregates inside the cell, making it difficult to reach a proper contrast for the images (in comparison to Fig. 1B control, where all the intracellular organelles are clearly stained) and originating some holes during the slicing procedure. The presence of large agglomerates of FLG is in line with the low dispersibility of FLG in aqueous-based media.[44]

We also observed the FLG flakes' morphology after being processed by the cells for extended periods. We incubated DRG neurons with 10 μg mL^{-1} of FLG for 24 h (representing the condition for maximum uptake). After replacing the medium and six further days of culture, cells were observed by TEM (Fig. 1D). Under these conditions, almost no holes were produced by the slicing procedure, and less internalized material was visible. In addition, the morphology appeared quite different, from flake-like after 24 h to amorphous carbon after 6 further days of cell processing. This might suggest the occurrence of some degradation phenomena, although data are not sufficient to conclude it definitively.

Biocompatibility of FLG on DRG neurons

Neuron viability upon FLG incubation at different concentrations was assessed through live calcein/propidium iodide (PI) staining to visualize both viable and dead neurons. Our data showed that the neuronal viability of FLG-treated neurons with respect to untreated neurons cultured under the very same conditions remained unchanged, even at high concentrations of FLG (Fig. 2A; Fig. S4†). Caspase3/7 staining was also performed to visualize the presence of apoptotic cells and to avoid an overestimation of neuron viability. The percentage of caspase-positive neurons remained below 2% under all experimental conditions, indicating the absence of apoptosis after FLG treatment (Fig. S5A–C†). Overall, no signs of cytotoxicity were observed after FLG exposure.

We also investigated the effects of prolonged contact with the lowest FLG concentration by assessing cell viability after 7 days (DIV11) of continuous GRM exposure. As can be observed in Fig. 2B, the viability after prolonged FLG exposure was not impaired over time, rather it slightly increased. This can be explained by the fact that DRG neurons tend to cluster in long-term cultures (Fig. S6A–D†) because of their intrinsic tendency to form a ganglion structure, becoming more resistant to the external environment. Therefore, after 7 days, the DRG neuron density in the selected fields was increased if compared to 24 h cultures (Fig. S6E†), resulting in a higher ratio of live over dead cells. These factors can explain the slight increase in viability observed after long-term exposure. Overall, under our experimental conditions, there are no particular concerns in the case of prolonged contact of DRG neurons to FLG.

There has been some evidence that the 3D structure of DRG neurons might be affected when they are under stressful

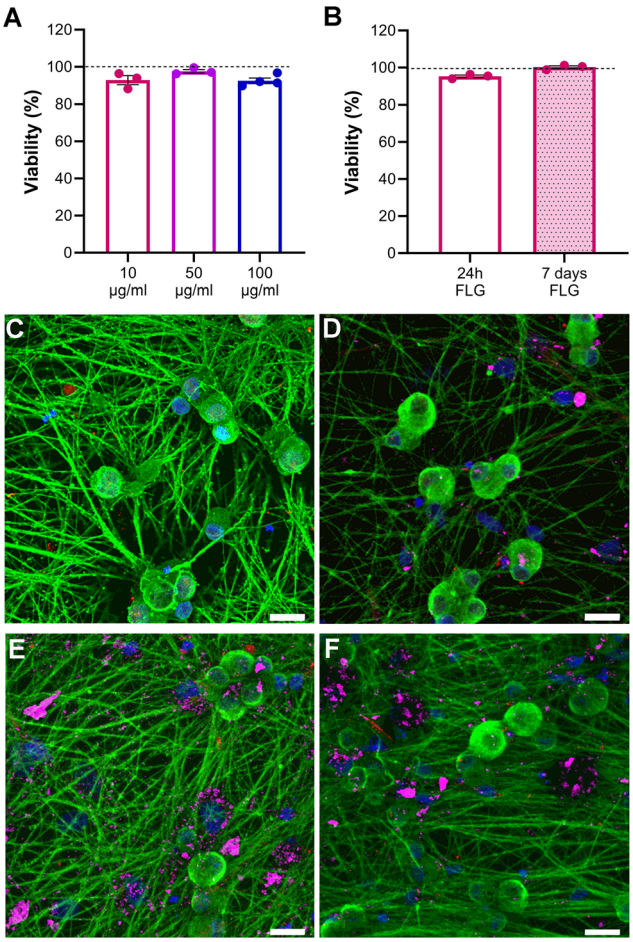

Fig. 2 Primary sensory neuron viability and morphology at different concentrations and times of exposure of FLG. (A) Normalized neuronal viability at 10 μg mL^{-1}, 50 μg mL^{-1} and 100 μg mL^{-1}. (B) Normalized neuronal viability after exposure to 10 μg mL^{-1} of FLG for 24 h and 7 days. Data are normalized over CTRL (100% viability; horizontal line) and expressed as means ± SEM, N = 3 (3/4 replicates). Statistical analysis was performed using Student's t-test for each condition. (C–F) Primary sensory neurons stained for the neuronal marker β-tubulin III (green), the glial marker α-GFAP (red), and nuclear stain DAPI (blue); CTRL (C), after incubation with 10 μg mL^{-1} (D), 50 μg mL^{-1} (E), and 100 μg mL^{-1} (F) of FLG (pink) for 24 h. Pictures taken at 63× magnification. Scale bars, 20 μm.

Open Access Article. Published on 09 Sunguti 2024. Downloaded on 2025-08-13 04:12:18.
This article is licensed under a Creative Commons Attribution-NonCommercial 3.0 Unported Licence.

conditions.[64,65] From optical observations, the neuronal morphology did not seem to be greatly affected after exposure to either concentration of FLG (Fig. 2C–E; Fig. S4†), as previously observed in SEM imaging (Fig. S2†). Confocal *z*-stack images were then acquired, allowing for the 3D reconstruction and calculation of the soma volume. It must be specified that, to perform this analysis, we selected DRG somas quite isolated from other cells. After exposure to either concentration of FLG, the cell body volume remained substantially unchanged (Fig. 3C; Fig. S7†). However, the shape of the soma was slightly affected after treatment with 100 μg mL^{-1} of FLG (Fig. 3A and B), with a significant increase in the average *Z*-length (Fig. 3D). To verify if most neurons with longer *Z*-lengths were, in general, larger, we calculated the cell volume to *Z*-length ratio. This ratio was significantly lower after FLG treatment, indicating that the effect was attributable to the change in neuron height (Fig. 3E). These morphological effects were concentration-dependent since the changes were only observed at high concentrations of FLG (Fig. S7†). The change in shape, but not in volume, might indicate an increase in soma elasticity, previously shown in DRG neurons suffering from sciatic nerve injury.[64] More research is needed to understand the basis of this phenomenon and the possible connection with cellular stress.

In Fig. S8,† we report a size distribution analysis performed on the diameters of the somas from 2D bright field (BF) images. From the analysis, it can be noticed that in untreated neurons, two main subpopulations can be identified, namely small/medium neurons (15–40 μm diameter) and medium/large (40–60 μm diameter). The size distribution differs from untreated controls when cells are exposed to increasing concentrations of FLG (Fig. S8B and C†). However, given the flakes' tendency to agglomerate over the cells (see Fig. S8A†), some of the smallest neurons might be lost in the analysis, being covered by the large black spot. Therefore, a significant effect of FLG on neuronal size and morphology cannot be fully demonstrated.

The internalization of FLG in DRG neurons did not show important signs based on the readouts analyzed so far. However, FLG might affect distinct intracellular pathways, resulting in functional changes. Therefore, proteomic analysis was performed on protein lysates from DRG neurons treated for 24 h with either 10 or 100 μg mL^{-1} of FLG (Fig. 4A and B).

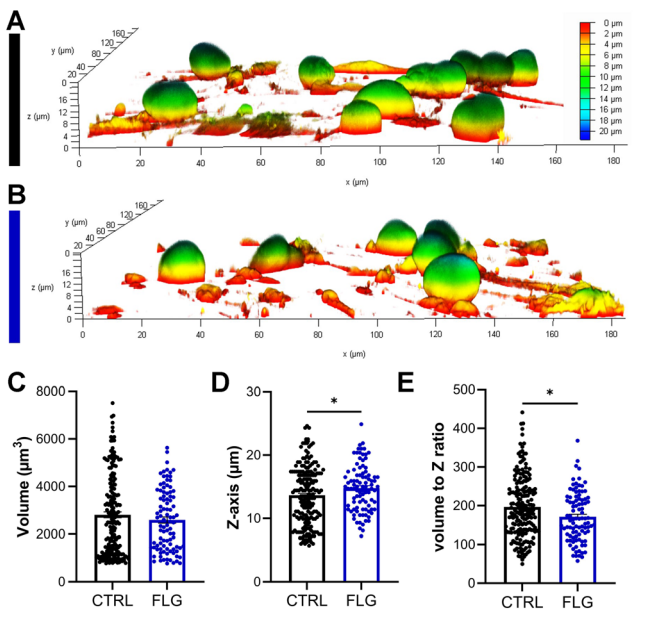

Fig. 3 3D analysis of DRG neurons after exposure to 100 μg mL^{-1} of FLG for 24 h. A and (B) Representative 3D side views of live DRG neurons with color coding based on neuron height (red low-blue high); (A) CTRL and (B) treated with 100 μg mL^{-1} FLG. (C) Neuron volume, (D) length of *Z*-axis as a measure of soma height, and (E) volume to *Z* ratio for CTRL neurons and FLG-treated neurons (100 μg mL^{-1}). Each point represents one neuron. All data are expressed as means ± SEM, $N = 3$ (6 replicates). Unpaired Student's *t*-test/Mann–Whitney *U*-test; *$p < 0.05$.

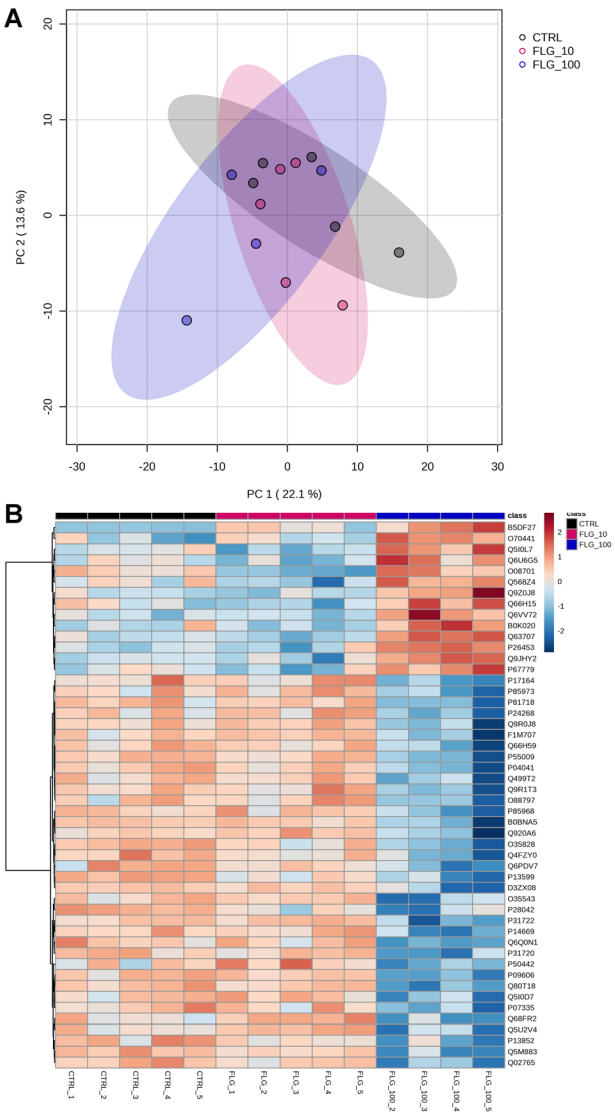

Fig. 4 Proteomics analysis. (A) PCA graph of CTRL *vs.* FLG-treated neurons at the concentrations of 10 and 100 μg mL^{-1}. (B) Heatmap of the 50 most significant proteins following ANOVA test.

This journal is © The Royal Society of Chemistry 2024

Open Access Article. Published on 09 Sunguti 2024. Downloaded on 2025-08-13 04:12:18.
This article is licensed under a Creative Commons Attribution-NonCommercial 3.0 Unported Licence.

However, PCA analysis of the proteomic data did not show a clear separation between CTRL and FLG clusters at both FLG concentrations (Fig. 4A).

Only for the high FLG concentration (100 μg mL^{-1}), the heatmap analysis reveals some significant changes in the protein expression (Fig. 4B). The figure shows the 50 most dysregulated proteins in FLG-treated DRG neurons as compared with CTRL neurons, 14 of which are significantly altered (ANOVA test, corrected p-value <0.05, see ESI files 1 and 2†). Gene ontology analysis indicates that this data are consistent with alterations in glutamate biosynthesis, collagen, and complement pathways (see ESI file 3†).

FLG does not affect the passive and active properties of DRG neurons

Besides viability, the passive and active electrical properties of DRG neurons are a very sensitive indicator of neuron health and function. In this context, we analyzed the single-cell neuronal properties of control DRG neurons and DRG neurons treated with low (10 μg mL^{-1}) and high (100 μg mL^{-1}) concentrations of FLG by measuring the whole-cell macroscopic currents (Fig. 5A). No significant differences were observed between the two groups in the outward current density (J; nA pF^{-1}) measured at 100 mV (Fig. 5C) using a ramp paradigm.

Patch-clamp recordings in current-clamp configuration were used to dissect the firing properties of DRG neurons in the experimental groups under study. To do this, we delivered constant current pulses (1 s duration) of increasing amplitude (in 10 pA steps) to evoke action potentials (APs) (Fig. 5B). Under these conditions, the initial resting membrane potential of treated and untreated DRG neurons was unchanged (Fig. 5D). Moreover, also the rheobase and the input resistance remained substantially unaffected by the FLG treatment (Fig. 5E and F).

To study in-depth the biophysical properties of the single AP, the plot of the time derivative of voltage (dV/dt) *vs.* voltage was constructed (phase-plot analysis).[66,67] The plot was obtained from the first AP elicited by the minimal current injection (rheobase) by current-clamp family step protocol (see Fig. 5B, inset). The following parameters were studied: threshold, AP peak, amplitude, and spike height. As seen in Fig. 5G–J, the presence of either 10 or 100 μg mL^{-1} FLG did not significantly affect these parameters of AP shape. Finally, the number of APs evoked as a function of current injection steps was also unaffected by FLG treatments (Fig. 5L).

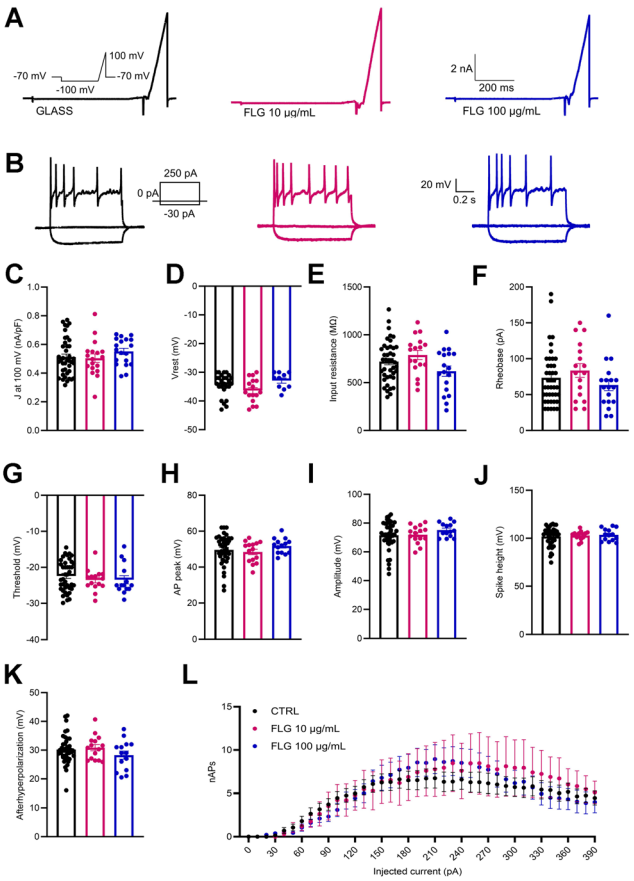

Fig. 5 (A) Representative whole-cell currents from control DRG (CTRL; black) and neurons treated with low (10 μg mL^{-1}, red) and high (100 μg mL^{-1}, blue) FLG concentrations. Macroscopic currents were elicited using a ramp stimulation (inset) with cells clamped at −70 mV before stimulation. (B) Representative current-clamp recordings of action potentials evoked by the injections of 10 pA step current (1 s duration, protocol shown in the inset) in the three experimental conditions. (C–K) Quantitative evaluation of the current density at 100 mV (CTRL, n = 40; FLG 10, n = 18; FLG 100, n = 19), resting membrane potential (CTRL, n = 27; FLG 10, n = 16; FLG 100, n = 10), input resistance, rheobase (CTRL, n = 41; FLG 10, n = 17; FLG 100, n = 18), threshold, AP peak and amplitude, AP spike height and afterhyperpolarization (CTRL, n = 40; FLG 10, n = 15; FLG 100, n = 14). (L) Number of APs generated by DRG neurons belonging to the three experimental conditions (CTRL, n = 41; FLG 10, n = 17; FLG 100, n = 18). Data are expressed as means ± SEM. One-way ANOVA/Tukey's tests or Kruskal Wallis/Dunn's test.

FLG increases the response of DRG neurons to noxious stimuli

DRG neurons are polymodal, detecting and responding to distinct noxious stimuli through a variety of specific receptors.[68] Since tissue acidification occurs under various painful conditions, primary sensory neurons express several acid sensors to detect changes in extracellular pH, such as acid-sensing ion channels (ASICs),[69] TRPV1,[70] proton-sensing G protein-coupled receptors, and two-pore domain potassium channels (K2P).[71,72] Thus, we investigated whether exposure of DRG neurons to FLG alters their physiological responses to noxious stimuli. When the response of DRG neurons to mild acidic pH (pH 6.0) was investigated, FLG-treated DRG neurons displayed similar responses to CTRL neurons in terms of both activated inward current and membrane depolarization (Fig. S9A and B†). Additional experiments were conducted to verify the DRG response to mechanical stress with or without FLG treatment. Specifically, we tested neurons for the increase in membrane surface tension produced by osmotic swelling in terms of change in inward/outward currents. As previously seen in response to acidic pH, treating cells with hypotonic solution increases whole-cell current recorded at 80/−80 mV evoked by

Open Access Article. Published on 09 Sunguti 2024. Downloaded on 2025-08-13 04:12:18.
This article is licensed under a Creative Commons Attribution-NonCommercial 3.0 Unported Licence.

ramp stimulation. This effect is likely due to a general activation of several mechano-sensitive channels expressed in DRG neurons, such as TRPV1,[73] TRPV4,[74] TRPA1,[75] TRPC5,[76] TRPM8,[77] TWIK-related spinal cord K^+ channel (TRESK) of the K2P family[78] and K^+–Cl^- cotransporter 3 (KCC3).[79] Under these conditions, no significant difference was found in inward/outward currents in CTRL and FLG-treated neurons (Fig. S9C†).

DRG neurons are also known to express several types of TRP channels that are implicated in a variety of sensory processes, such as thermosensation, mechanosensation, osmosensation, olfaction, taste, and pain perception.[80,81] In particular, two key chemoreceptors identified in these neurons are the TRPV1, the receptor for "hot" compounds in different types of pepper,[82–84] and TRPA1, the receptor for pungent compounds, such as mustard oil and cinnamon, that are expressed in small/medium neuronal subgroup.[85,86] Consequently, we investigated whether the treatment with 10 μg mL^{-1} FLG alters the response of these two nociceptors in DRG neurons.

To investigate DRG responses mediated by TRPV1 channels, we used the agonist capsaicin (Fig. 6A). Interestingly, when we measured the capsaicin-dependent inward current at negative potentials (−70 mV) using whole-cell patch-clamp in voltage-clamp configuration, we observed a significantly increased response of neurons treated with FLG, compared with the control group (Fig. 6B–D). The specificity of the effect was assessed using capsazepine, a selective antagonist of the TRPV1 channel, that effectively blocked the inward current in both CTRL and FLG-treated neurons (Fig. 6D). In addition, current-clamp recordings showed that the observed increase in the capsaicin-evoked inward current at negative potentials was associated with a sustained depolarization of the membrane potential of FLG-treated DRG neurons (Fig. 6D).

We also investigated the effect of FLG treatment on the responses of DRG neurons mediated by TRPA1 channels. To this purpose, we administered allyl isothiocyanate (AITC), a specific TRPA1 agonist, to DRG neurons in the presence and absence of FLG treatment (Fig. 7A). When the current density/voltage (J/V) relationships of the TRPA1-mediated current activated by AITC were studied in CTRL and FLG-treated DRG neurons using a ramp protocol (Fig. 7B), a significantly increased response was again observed in DRG-treated neurons compared to CTRL neurons, at both at +80 and −80 mV holding potentials (Fig. 7C and D). The specificity of the response for TRPA1 channels was assessed by using, under the same conditions, HC03003, a selective TRPA1 channel blocker, that fully abolished the AITC-induced current in both CTRL and FLG-treated neurons (Fig. 7E).

Taken together, all these results show that in the presence of both low and high FLG concentrations, the functionality of DRG neurons does not change in terms of acidic pH sensitivity, macroscopic currents, and firing properties. However, when we looked at the functionality of DRG neurons sensitive to specific irritant modalities, we found an increased response in DRG neurons treated with a low concentration of FLG.

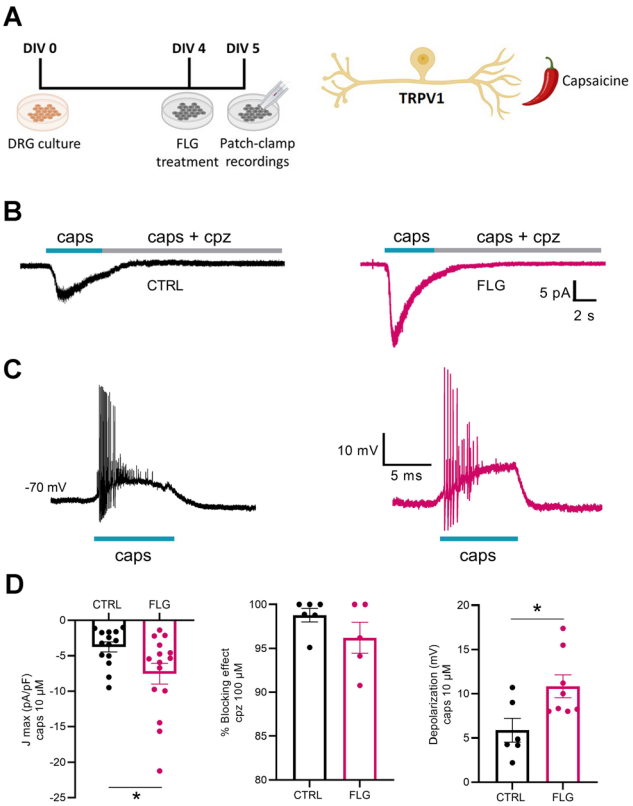

Fig. 6 (A) Timeline of the experiments (left) and cartoon of the TRPV1-specific agonist capsaicin used for electrophysiological recordings (right). (B) Representative TRPV1 inward current evoked by capsaicin (caps, 10 μM) and blocked by capsazepine (cpz, 100 μM) at a holding potential of −70 mV in control untreated neurons (CTRL; black) and FLG-treated neurons (10 μg mL^{-1}; pink). (C) Representative current clamp recordings of TRPV1-dependent membrane depolarization studied in CTRL and FLG-treated neurons. (D) Current density (left) and net percent effect of capsazepine blockade (center) on capsaicin-induced TRPV1 activation recorded in CTRL and FLG-treated neurons, studied as in B (CTRL = 14, FLG = 15 for J, and CTRL, n = 6; FLG, n = 5, for cpz block). Quantitative evaluation of the extent of depolarization elicited by capsaicin in CTRL and FLG-treated DRG neurons, studied as in C (CTRL, n = 6; FLG, n = 8) (right). Data are expressed as means ± SEM. Unpaired Student's t-test; *p < 0.05.

As mentioned, TRP channels are highly expressed in a subset of small/medium diameter DRG neurons,[80] the same subtypes analyzed in the electrophysiological experiments, and are a major integrator of noxious stimuli, ranging from exogenous chemical agents (capsaicin) to endogenous agonists (*e.g.*, acidic and basic pH).[87] To understand whether the observed effects were due to an increase of channel expression or to an increased responsivity of FLG-treated neurons to the stimulus, we looked at the TRPV1 expression by DRG neurons under our experimental conditions. When compared to control DRG neurons, FLG-treated neurons did not show a clear-cut overexpression of TRPV1/TRPA1 channels, nor a tendency of the channels to translocate from the membrane to the intracellular compartment (Fig. S10 and S11†). Proteomics data were also unable to uncover a clear upregulation of TRPV1 and TRPA1

This journal is © The Royal Society of Chemistry 2024

Open Access Article. Published on 09 Sunguti 2024. Downloaded on 2025-08-13 04:12:18.
This article is licensed under a Creative Commons Attribution-NonCommercial 3.0 Unported Licence.

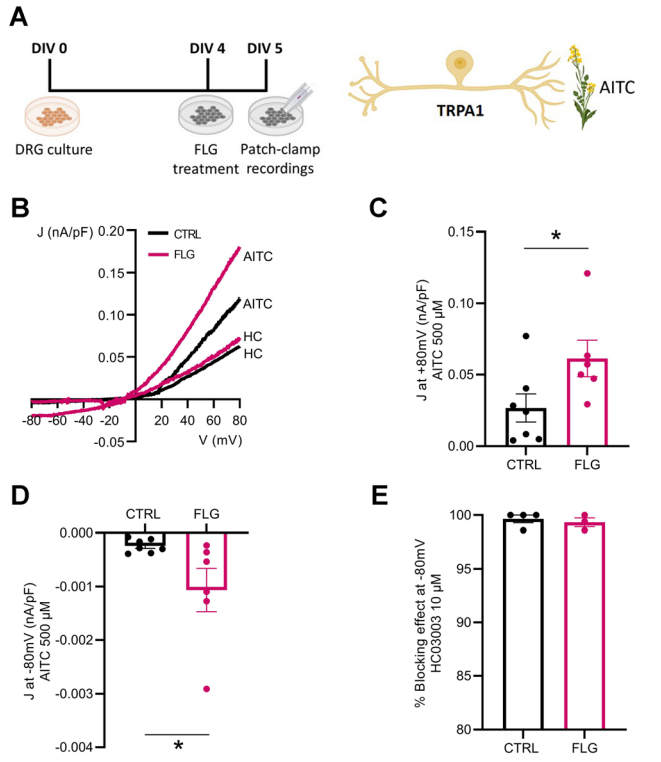

Fig. 7 (A) Timeline of the experiments (left) and cartoon of the TRPA1-specific agonist allyl isothiocyanate (AITC, 500 µM) used for the electrophysiological recordings (right). (B) Current density/voltage (*J*/*V*) relationships of TRPA1 channel activated by AITC in control untreated (CTRL) and FLG-treated (10 µg mL^{-1}) DRG neurons. (C) and (D) Quantitative evaluation of whole-cell currents recorded at +80 mV and −80 mV in CTRL and FLG-treated neurons (CTRL, n = 7; FLG, n = 6). (E) Quantitative evaluation of the net percent effect of HC03003 (10 µM) blockade on AITC evoked currents under both conditions studied (CTRL, n = 4; FLG, n = 3). Data are expressed as means ± SEM. Unpaired Student's t-test; *p < 0.05.

channels. This can be due to the large heterogeneity of neuronal subtypes and the presence of glial cells that will dilute out alterations in the single-cell population on which electrophysiological recordings were performed. However, our data suggest that the increase of TRP-mediated currents in FLG-treated neurons is attributable to an increased membrane exposure of the cellular TRP pool or an enhancement of channel sensitivity to the agonists. The latter explanation is in line with the proteomics data of increased complement activation in FLG-treated neurons that might imply an increased sensitization of the nociceptive neurons (ESI file 3†). Additional research is needed to explain why FLG increases the activity of DRG neurons in response to certain physiological stimuli and to fathom the importance and the consequences of this effect.

Materials and experimental design. The study was designed to gain insight into the effects of colloidal FLG exposure on DRG neurons *in vitro*. FLG was prepared and characterized by a collaborating laboratory at the University of Castilla-La Mancha (UCLM; Spain), and the characterization was extensively described in our previous works.[58,88] The graphene flakes were dissolved in MilliQ water and sonicated (frequency 37 Hz, power 100%, 10 min using a Fisherbrand 112xx series sonicator) before each experimental use. Primary DRG neurons were obtained from P2/P3 rat pups (Charles River, Calco, Italy). On DIV4, GRMs were added to the neurons.

Preparation of primary sensory neuron cultures. All experiments were carried out in accordance with the guidelines established by the European Community Council (Directive 2010/63/EU of 22 September 2010) and were approved by the Italian Ministry of Health. All efforts were made to minimize animal numbers and suffering. A total of 4/6 pups was used for each dissection.

Primary sensory neuron cultures were prepared from wild-type P2/P3 Sprague-Dawley rat pups (Charles River, Calco, Italy). The DRGs were dissected out, dissociated, and cultured with a protocol optimized in-house.[89,90] We prepared two types of medium to be used during dissociation. The *dissociation medium* consisted of Neurobasal (Gibco, Thermo Fisher Scientific, Massachusetts, USA) supplemented with fetal bovine serum (10%, FBS, Thermo Fisher Scientific) and penicillin/streptomycin (50 U mL^{-1}, Sigma-Aldrich, Missouri, USA). The *growth medium* consisted of Neurobasal supplemented with Pen/Strep (50 U mL^{-1}), recombinant human β-NGF (50 ng mL^{-1}, Bio-Techne, Minnesota, USA), BSA (0.05%), B-27 (2%, Thermo fisher scientific) and Glutamax (1%, Thermo Fisher Scientific).

After sacrificing the pups by decapitation, we made an incision from head to tail following the ribcage. We peeled the skin, cut out all organs, and trimmed the vertebrae to free up the spinal column. Once the spinal column was cut out, we used hydraulic extrusion to remove the spinal cord.[90] We then cut through the ventral and dorsal columns to obtain two separate parts of the spinal column, each containing 15 DRGs. DRGs were now visible and ready to be extracted from their pockets. They were freed of excess nerve roots and meninges and washed in HBSS (Hank's Balanced Salt Solution, Sigma-Aldrich).

After the isolation of the DRGs, the dissociation could start. HBSS was removed and replaced by Trypsin–EDTA (0.05%, TE, Thermo Fisher Scientific), and DRGs were incubated for 20 min at 37 °C. Then, DRGs were collected in a 50 ml Falcon tube using a flamed Pasteur glass pipet and TE in the dissociation medium. DRGs were spun down at 200*g* for 2 min, and the supernatant was removed and replaced by collagenase (0.1%, Type 1, Sigma-Aldrich) for a 90 min dissociation at 37 °C. After this second dissociation step, collagenase was neutralized and removed by centrifugation (200*g*, 3 min). One mL of dissociation medium was added to the pellet, and DRGs were mechanically dissociated by triturating 6–10 times using a flamed glass Pasteur pipet. This was again centrifuged (200*g*, 5 min) and the dissociation medium was replaced by 1 mL of growth medium. DRGs were further mechanically dissociated until no DRGs were visible. Dissociated cells were spotted onto laminin/poly-D-lysine (PDL) (Mouse Laminin, Sigma; PDL, Sigma) coated glass coverslips, in 6- or 12-well plates (Falcon,

Open Access Article. Published on 09 Sunguti 2024. Downloaded on 2025-08-13 04:12:18.
This article is licensed under a Creative Commons Attribution-NonCommercial 3.0 Unported Licence.

Corning, NY, USA). After 1 h incubation to allow cells to attach, the well was flooded with the appropriate amount of medium. The final cell density was 100 000 cells per mL. To reduce the presence of glial cells, the antimitotic cytosine β-D-arabinoside (final concentration of 1 μM) was added after 24 h and again at DIV4. This treatment was done by replacing half of the medium with fresh growth medium containing 2 μM cytosine β-D-arabinoside.

FLG treatment was initiated at DIV4 by replacing half of the medium with fresh growth medium containing either FLG at the desired concentration or H_2O (CTRL). Neurons were exposed to graphene for a minimum of 4 h to a maximum of 7 days, at concentrations ranging from 10 to 100 μg mL^{-1}. After exposure, DRG neurons were interrogated in terms of morphology, viability, proteomics, and electrophysiological properties.

Cell viability assay. After graphene incubation, neurons were stained for 5 min at room temperature (RT) with propidium iodide (PI, 1 μM) for cell death quantification, calcein–AM (1 μM) for cell viability, and Hoechst33342 (1 μM) for nuclear visualization. Cell viability was quantified at 10× magnification using a Nikon Eclipse-80i upright epifluorescence microscope (Nikon, Tokyo, Japan). Six fields were randomly selected per sample. Image analysis was performed using the Cell Counter plugin of ImageJ software.

Caspase 3/7 analysis. After graphene incubation, neurons were stained for 30 min at 37 °C with Caspase 3/7 (Thermo Fisher Scientific, C10423, 1/1000 in culture medium). At the end of the incubation, the medium was replaced with PBS supplemented with PI (1 μM) and Hoechst33342 (1 μM) and further incubated for 5 min. Caspase activity was quantified at 10× magnification using a Nikon Eclipse-80i upright epifluorescence microscope (Nikon, Tokyo, Japan). Each sample was scanned completely for the presence of caspase-positive cells. Image analysis was performed using the Cell Counter plugin of ImageJ software.

Uptake analysis by flow cytometry. For flow cytometry analysis, neurons were detached by incubating them with TE (0.05%) for 2 min at 37 °C. Upon cell detachment, the TE was neutralized with cell medium and the detached cells were pelleted by centrifugation (5 min, 200*g* at RT). Pellets were resuspended in 200 μl 1× phosphate-buffered saline (PBS) and collected in round bottom polystyrene tubes. Propidium iodide (PI; 1 μM) was added to label dead cells. Cell suspensions were run on a MaxQuant Analyzer 10 (Miltenyi) flow cytometer and analyzed with Flow Jo 10.8. Flow cytometry analysis involved doublets, cell debris and dead cell exclusion through gating. SSC median values were considered before and after dead cells exclusion.

Immunofluorescence staining. For immunofluorescence analysis, DRG neurons were first fixed in paraformaldehyde (4%, PFA) for 15 min at RT. Then, neurons were permeabilized with 0.1% Triton X-100 for 5 min, followed by 30 min blocking in BSA (2%). After 3 washes with 1× PBS, neurons were incubated for 3 h at RT with primary antibodies, diluted 1 : 200 in 2% BSA. The primary antibodies used were rabbit polyclonal anti-β-tubulin III (Sigma Aldrich, T2200) and guinea pig polyclonal anti-GFAP (SYSY, 173004). Subsequently, neurons were washed 3 times in 1× PBS and incubated for 1 h at RT with secondary antibodies diluted 1 : 500 in BSA (2%). The fluorescently conjugated secondary antibodies were labeled by Alexa Fluor 488 or Alexa Fluor 568 (#11029 and #A11036, respectively; ThermoFisher Scientific, Molecular Probes). Finally, after another washing round, neurons were stained with Hoechst33342 diluted 1 : 100 in BSA (2%) for 5 min.

For studies on the channel distribution, polyclonal anti-TRPV1 (ACC-334, Alomone labs) and TRPA1 (ACC-037, Alomone labs) were used, and the permeabilization step with 0.1% Triton X-100 was not performed, in order to bind only to the extracellular domain. The stained coverslips were mounted in Vectashield (H-1000-10; Vector Laboratories, Newark, USA) on 1 mm thick microscope slides. *Z*-Stack image acquisition was performed using a confocal microscope (SP8, Leica Microsystems GmbH, Wetzlar, Germany) at 63× (1.4 NA) magnification.

Protein extraction. Protein extraction was performed prior to mass spectrometry analysis. First, the medium was removed, and the neurons were washed 3× in PBS. Then, the cells were lysed by replacing the PBS with RIPA buffer (10 mM Tris-HCl pH 7.4, 140 mM NaCl, 1 mM EDTA, 0.5 mM EGTA, 1% Triton X-100, 0.1% sodium dodecyl sulfate and 0.1% sodium deoxycholate) supplemented with proteases inhibitors (complete EDTA-free protease inhibitors, Roche Diagnostic, Monza, Italy) and phosphatases inhibitors (serine/threonine phosphatase inhibitor and tyrosine phosphatase inhibitor, Sigma) and subsequently scraping the cells off. The lysates were sonicated for 10 s using a BRANSON SLPe (25% amplitude) and centrifuged for 15 min (4 °C, at 19 000*g*). The supernatants were collected, and the total protein content was determined with the BCA Protein Assay kit (Thermo Fisher Scientific) using the standard protocol.

Surface biotinylation assays. Twenty-four hours after the treatment, DRG neurons were washed 3× in PBS and incubated with 1 mg mL^{-1} of EZ-Link™ Sulfo–NHS–LC–biotin (Thermo Fisher Scientific) in cold phosphate-buffered saline (PBS) pH 8 for 30 min at 4 °C under constant mixing. Cells were washed 2× with 50 mM Tris pH 8 and 2× with cold PBS pH 8 to remove the excess biotin before being lysed with RIPA buffer (10 mM Tris-HCl pH 7.4, 140 mM NaCl, 1 mM EDTA, 0.5 mM EGTA, 1% Triton X-100, 0.1% sodium dodecyl sulfate and 0.1% sodium deoxycholate) supplemented with proteases inhibitors (complete EDTA-free protease inhibitors, Roche Diagnostic, Monza, Italy) and phosphatases inhibitors (serine/threonine phosphatase inhibitor and tyrosine phosphatase inhibitor, Sigma).

Total cell lysates were centrifuged at 10 000*g* at 4 °C for 10 min. An aliquot of supernatant fractions was kept for the input (total) sample, while the remaining fraction was incubated with 100 μl of NeutrAvidin-conjugated agarose beads (Thermo Fisher Scientific) at 4 °C for 3 h. Supernatants containing intracellular proteins were collected, and the beads were washed 2× in RIPA buffer and 2× in PBS prior to samples (membrane proteins) elution.

 This journal is © The Royal Society of Chemistry 2024

Open Access Article. Published on 09 Sunguti 2024. Downloaded on 2025-08-13 04:12:18.
This article is licensed under a Creative Commons Attribution-NonCommercial 3.0 Unported Licence.

Western blotting analysis. Western blotting analysis was performed to determine the amount of TRPV1 and TRPA1 proteins expressed by treated and untreated DRG neurons. From each condition, total, intracellular and extracellular fractions were separated by maxi sodium dodecyl sulfate-polyacrylamide gel electrophoresis (MAXI SDS-PAGE). The stacking and running gels were prepared at 5% and 8% acrylamide, respectively. All proteins were denatured for 5 min at 70 °C prior to gel loading. After successful separation, proteins were transferred onto a nitrocellulose membrane (Amersham Protran, Cytiva) overnight at 150 mA. Subsequently, a blocking step with 5% milk in Tris-buffered saline containing 0.05% Tween-20 (0.05% TBS-T) for 1 h at room temperature was performed to reduce non-specific binding. Next, the membrane was incubated overnight with antibodies against: TRPV1 (rabbit polyclonal, Alomone Labs, ACC-030, 1/500), TRPA1 (rabbit polyclonal, Thermo Fisher Scientific, PA1-46159, 1/500), and the housekeeping proteins GAPDH (rabbit polyclonal, Abcam 9485, 1/5000) and Na^+/K^+ ATPase α-1 (mouse monoclonal, Millipore, 05-369, 1 : 2000). After washing with 0.05% TBS-T, the membrane was incubated with HRP-conjugated secondary antibodies (Abcam, 1 : 5000) for 1 h at RT. The secondary antibodies were washed away in 0.05% TBS-T, and the membrane was developed using the ECL Prime Western Blotting System (Amersham Protran, Cytiva). The chemiluminescent signals were revealed using the iBright FL1500 Imaging System (Thermo Fisher Scientific, A44241), and band intensities were analyzed with iBright Analysis Software. Since TRPV1 and Na^+/K^+ ATPase α-1 have similar molecular weights, after the first acquisition, the nitrocellulose membranes were washed to remove the chemiluminescent substrate and incubated in Restore Western Blot Stripping Buffer (Thermo Fisher Scientific) for 20 min to remove primary and secondary antibodies, washed in 0.05% TBS-T and tested for removal of antibodies before performing the next immunoblot experiments.

Mass spectrometry. For each condition, 50 μg of protein lysate was used for proteomics analysis. A QC sample (pool of 25 samples) was acquired to ensure the quality of data. The tryptic peptides, after undergoing trapping and desalting, were loaded on an Aurora C18 column (75 mm × 250 mm, 1.6 μm particle size) nanocolumn (Ion Opticks, Fitzroy, Australia). Peptides were separated using a linear gradient of acetonitrile in water (with 0.1% formic acid), from 3% to 95% over the course of 45 min, followed by column cleaning and reconditioning. This was conducted on a Thermo Exploris 480 orbitrap system, coupled with a Dionex Ultimate 3000 nano-LC system. The flow rate was set to 300 nL min^{-1}, the injection volume to 1 μL, and the total run time was 1 h. All peptides were analyzed in positive ESI mode, using a capillary voltage set to 2.0 kV. The RF lens was set to 40%, and the AGC target was set to 300%. Data acquisition was performed in Data Independent mode (DIA) with a survey scan set from 400 to 1000 m/z at 120 000 resolution, followed by MS/MS acquisition of 60 m/z transmission windows, each with a fixed 10 Da width. MS/MS spectra were acquired in HCD mode. The MS/MS spectra were analyzed using Spectronaut,[91] by running a DirectDIA analysis against the reference *Rattus* FASTA database (Tax ID: 10 114 reporting 17 126 reviewed entries). Cysteine carbamidomethylation was selected as a fixed modification; acetylation, methylation, deamination, oxidation, and phosphorylation were selected as variable modifications. Positive protein identifications were retained at 1% false discovery rate (FDR) threshold and at least two peptides were used for protein quantification. Features with CV (coefficient of variation) > 30% in the QC samples were removed. The final data set was analyzed using the free on line software Metaboanalyst.[92] Features with more than 50% of missing values were removed, data were normalized by sum, Log-transformed and Pareto scaled. Gene Ontology analysis was performed using STRING.[93]

3D neuron morphometry. To determine the cell volume, DRG neurons were stained with calcein and live analyzed. *Z*-Stack image acquisition was performed using a confocal microscope (SP8, Leica Microsystems GmbH, Wetzlar, Germany) at 63× (1.4 NA) magnification. The images were then analyzed on CellProfiler, employing a single cells 3D analysis pipeline. Briefly, the cells were segmented based on the calcein signal, and the *Z*-axis length and volume were computed.[94]

Transmission electron microscopy (TEM). TEM imaging was performed to visualize GRM nanosheets directly inside the neurons. Neurons were detached using the same protocol used for flow cytometry and pelleted by gentle centrifugation (200*g*, 5 min). Fixation was performed in three separate steps. First, neurons were fixed in a growth medium containing glutaraldehyde (2%) for 45 min. Then, they were fixed in 0.1 M sodium cacodylate buffer at pH 7.4 containing glutaraldehyde (2%) for 1 h. After this fixation, neurons were washed 3 times in sodium cacodylate buffer. The last fixation step was in sodium cacodylate buffer containing osmium tetroxide (1%) for 1 h. Next, neurons were stained with an aqueous solution containing uranyl acetate (1%). After progressive dehydration in increasing percentages of ethanol, cells were embedded in epoxy resin (Epon 812, TAAB) and sliced using a diamond blade (Diatom) with an ultramicrotome (UC6, Leica). TEM micrographs were obtained using a JEOL JEM 1011, 100 kV acceleration voltage.

Scanning electron microscopy (SEM). DRG neurons were fixed for SEM at DIV5. Samples were rinsed 3× in PBS and then fixed with glutaraldehyde (2% v/v) in sodium cacodylate buffer (0.1 M) for 2 h at RT. The fixed DRG neurons were washed in cacodylate buffer (0.1 M) for 10 min. This was repeated another 2×, followed by two washes in MilliQ water for 5 min. Following these washing steps, samples were subjected to sequential dehydration in graded ethanol (30, 50, 70, 90, 96 and 100% v/v). Each percentage was used twice. After dehydration, samples were rinsed in a solution of hexamethyldisilazane (HMDS) and ethanol at increasing HMDS concentrations (25, 50 and 75% v/v) for 10 min each. At last, the cells were incubated in pure HMDS for 30 min and left overnight to evaporate overnight under the fume hood. Unless otherwise indicated, all chemicals were purchased from Sigma Aldrich.

Open Access Article. Published on 09 Sunguti 2024. Downloaded on 2025-08-13 04:12:18.
This article is licensed under a Creative Commons Attribution-NonCommercial 3.0 Unported Licence.

Patch-clamp recordings. Whole-cell patch-clamp recordings from sensory DRG neurons were carried out 5 days after seeding on 25 mm Ø glass coverslips as previously described.[84] For whole-cell voltage-clamp of inward/outward currents and current clamp recordings of firing activity, cells were continuously bathed using Tyrode external solution containing (in mM): NaCl 140, $CaCl_2$ 2, $MgCl_2$ 1, Glucose 10, HEPES 10, pH 7.3 with NaOH. The osmolality of the isotonic solution was 296 mOsm kg^{-1}. A hypotonic bath solution was made by decreasing NaCl to 95 mM (210 mOsm kg^{-1}). Borosilicate glass pipettes were pulled to a resistance of 4–5 MΩ when filled with an internal solution containing (in mM): 4 NaCl, 126 K gluconate, 0.02 $CaCl_2$, 1 $MgSO_4$, 5 HEPES, 15 glucose, 3 ATP, 0.1 GTP and 0.1 BAPTA, pH 7.2 with KOH. Recordings in dissociated neurons were restricted to small DRG neurons (capacitance <15 pF). After achieving a gigaseal and whole-cell configuration, macroscopic currents were elicited using a 200 ms hyperpolarization step to −100 mV followed by a 200 ms linear ramp up to 100 mV. All recordings were performed by clamping the cell under study at a holding potential of −70 mV. Capsaicin, capsazepine and HC030031 were dissolved in DMSO at a concentration of 10 mM. AITC was dissolved in ETOH at a concentration of 100 mM. All substances were diluted to the concentration of use in an external solution on the same day of the experiment. The different drug solutions were applied with a gravity-driven, local perfusion system at a flow rate of about 200 µl min^{-1} positioned within 100 µm of the neuron under study. The current density (J) was obtained by dividing the peak current by the cell capacitance (nA pF^{-1}). Current-clamp recordings of neuronal firing activity and the following analysis were performed as previously described.[66,67] Neuronal cells were held at a potential of −70 mV and APs were induced by injection of 10 pA current steps of 1 s. The resting membrane potential was measured after switching to current-clamp at I = 0 pA. To study firing activity, the current injection was adjusted to obtain an initial membrane potential of −70 mV before stimulation. To study the biophysical properties of the single AP, the plot of the time derivative of voltage (dV/dt) *vs.* voltage was constructed (phase-plane plot).[66,67] This plot was obtained starting from the first AP elicited by minimal current injection. The rheobase was calculated as the minimum depolarizing current needed to elicit at least one AP. Input resistance was calculated in the linear region of the voltage–current relationship determined after the injection of hyperpolarizing and depolarizing current steps (−20, −10, 10, 20 pA). The voltage threshold was defined as the first voltage value at which dV/dt exceeded 4 mV ms^{-1}. The peak amplitude of APs was measured from the voltage threshold to the AP peak. The spike height was defined as the peak relative to the most negative voltage reached during the afterhyperpolarization immediately after the spike. The afterhyperpolarization was determined as the difference between the most negative voltage reached during the hyperpolarization immediately after the spike and the threshold value. Current-clamp recordings of the firing activity of low-density DRG neurons were sampled at 50 kHz and low-pass filtered at 10 kHz. Recordings with leak currents >200 pA or series resistance >20 MΩ were discarded. Data acquisition was performed using the PatchMaster program (HEKA Elektronic) and the offline analysis was performed by Fit Master (HEKA Elektronic) software. Series resistance was compensated 80% (2 µs response time) and the compensation was readjusted before each stimulation. All recordings were performed at room temperature.

Statistical analysis. Data were analyzed by using Prism Software. '*N*' indicates the number of dissections, 'replicates' indicates the different glass slides within one dissection, and '*n*' indicates the number of neurons per group. All viability and flow results were normalized to CTRL. The normal distribution of data was assessed using the D'Agostino–Pearson's normality test. To compare two normally distributed sample groups, the unpaired Student's *t*-test was used. To compare two sample groups that were not normally distributed, the non-parametric Mann–Whitney *U*-test was used. To compare more than two normally distributed sample groups, one-way ANOVA was used, followed by Tukey's multiple comparisons test. In cases in which more than two sample groups were not normally distributed, the Kruskal-Wallis' test was used, followed by the Dunn's multiple comparison test. All data are expressed as means ± SEM with superimposed the individual experimental points.

Conclusions

In conclusion, our data show excellent FLG biocompatibility towards DRG sensory neurons. Upon incubations with different FLG concentrations (10–100 µg mL^{-1}), for various incubation times (1–7 days), neuronal viability, morphology, protein content, and basic electrical properties were preserved. Graphene flakes appear to be actively internalized and accumulated in large intracellular vesicles and possibly degraded over time.

For the higher FLG concentration (100 µg mL^{-1}), we observed mild morphological changes and protein dysregulation related to the glutamate signaling pathway and collagen. Glutamate is an essential neurotransmitter in the nervous system, and its upregulation can cause overexcitation of the neurons. Collagen also plays a pivotal role in peripheral nerves for Swann cell differentiation and nerve regeneration.[88] This might be important when graphene is employed as a scaffold for nerve regeneration after injury. The complement pathway was also found to be upregulated, which in normal circumstances can lead to inflammatory damage, but in the case of nerve injury, it can stimulate nerve regeneration and sensitization of nociceptive neurons.[95]

Interestingly, in our electrophysiological investigation under noxious stimuli, we observed an increased functional response upon FLG treatment of the nociceptive subpopulation of DRG neurons in response to irritants specific for the TRPV1 and TRPA1 chemoreceptors involved in sensing acute noxious, mechanical, and chemical stimuli, as well as in neu-

 This journal is © The Royal Society of Chemistry 2024

Open Access Article. Published on 09 Sunguti 2024. Downloaded on 2025-08-13 04:12:18.
This article is licensed under a Creative Commons Attribution-NonCommercial 3.0 Unported Licence.

ropathic pain. Considering the present findings, the setup of future applications of FLG in regenerative medicine, tissue engineering, and drug delivery should consider the potential interference of this material with the physiology of these channels. Even when employed in planar substrates, if subjected to biological and mechanical stress, graphene can undergo aging and delamination over time. Therefore, the possibility should be considered that FLG flakes, in contact with sensory neurons, could lower their activation threshold (sensitization) and induce an increase in the perception of irritant stimuli. On the other hand, our work could potentially open up novel routes for applications of bare graphene materials. Further investigation of their specific role in sensory neurons' overactivation might introduce the use of these materials under conditions in which nociception is impaired.

Author contributions

L. D., F. F., M. T., N. L.: investigation, formal analysis; L. D. writing; D. D.: investigation; E. V.: resources; S. V., F. L., A. A., V. C.: Formal analysis; P. V., V. C., F. B.: conceptualization, supervision, writing, review, and editing.

Conflicts of interest

There are no conflicts to declare.

Acknowledgements

We thank Ilaria Dallorto, Rossana Ciancio, Diego Moruzzo, and Arta Mehilli, and Antonella Marte for administrative and technical help. The project has received funding from: the European Union's Horizon 2020 Research and Innovation Programme under Grant Agreement No. 881603 Graphene Flagship, Core 2 and Core 3 (to F. B.); the Italian Ministry of Foreign Affairs and International Cooperation (grant agreement no. MAE00694702021-05-20 to F. B.); IRCCS Ospedale Policlinico San Martino, Genova, Italy (Ricerca Corrente and "5 × 1000" to F. B. and V. C.).

References

1 K. S. Novoselov, A. K. Geim, S. V. Morozov, D. Jiang, Y. Zhang, S. V. Dubonos, I. V. Grigorieva and A. A. Firsov, *Science*, 2004, **306**, 666–669.
2 K. S. Novoselov, D. Jiang, F. Schedin, T. J. Booth, V. V. Khotkevich, S. V. Morozov and A. K. Geim, *Proc. Natl. Acad. Sci. U. S. A.*, 2005, **102**, 10451–10453.
3 A. K. Geim, *Science*, 2009, **324**, 1530–1534.
4 Y. Zhang, T. R. Nayak, H. Hong and W. Cai, *Nanoscale*, 2012, **4**, 3833–3842.
5 J. Byun, *J. Microbiol. Biotechnol.*, 2015, **25**, 145–151.
6 D. Chimene, D. L. Alge and A. K. Gaharwar, *Adv. Mater.*, 2015, **27**, 7261–7284.
7 V. C. Sanchez, A. Jachak, R. H. Hurt and A. B. Kane, *Chem. Res. Toxicol.*, 2012, **25**, 15–34.
8 K. Kostarelos and K. S. Novoselov, *Science*, 2014, **344**, 261–263.
9 M. Bramini, G. Alberini, E. Colombo, M. Chiacchiaretta, M. L. DiFrancesco, J. F. Maya-Vetencourt, L. Maragliano, F. Benfenati and F. Cesca, *Front. Syst. Neurosci.*, 2018, **12**, 12.
10 J. W. Jeong, G. Shin, S. I. Park, K. J. Yu, L. Xu and J. A. Rogers, *Neuron*, 2015, **86**, 175–186.
11 V. S. Polikov, P. A. Tresco and W. M. Reichert, *J. Neurosci. Methods*, 2005, **148**, 1–18.
12 M. P. Ward, P. Rajdev, C. Ellison and P. P. Irazoqui, *Brain Res.*, 2009, **1282**, 183–200.
13 K. Scholten and E. Meng, *Lab Chip*, 2015, **15**, 4256–4272.
14 A. Halim, K. Y. Qu, X. F. Zhang and N. P. Huang, *ACS Biomater. Sci. Eng.*, 2021, **7**, 3503–3529.
15 J. Chen, H. Liu, C. Zhao, G. Qin, G. Xi, T. Li, X. Wang and T. Chen, *Biomaterials*, 2014, **35**, 4986–4995.
16 S. R. Shin, Y. C. Li, H. L. Jang, P. Khoshakhlagh, M. Akbari, A. Nasajpour, Y. S. Zhang, A. Tamayol and A. Khademhosseini, *Adv. Drug Delivery Rev.*, 2016, **105**, 255–274.
17 Z. Li, W. Zhang and F. Xing, *Int. J. Mol. Sci.*, 2019, **20**(10), 2461.
18 H. Zhang, T. Fan, W. Chen, Y. Li and B. Wang, *Bioact. Mater.*, 2020, **5**, 1071–1086.
19 X. Wang, M. Guo, Y. Liu, K. Niu, X. Zheng, Y. Yang and P. Wang, *ACS Appl. Bio Mater.*, 2021, **4**, 4236–4243.
20 Y. Zheng, X. Hong, J. Wang, L. Feng, T. Fan, R. Guo and H. Zhang, *Adv. Healthc. Mater.*, 2021, **10**, e2001743.
21 M. Aleemardani, P. Zare, A. Seifalian, Z. Bagher and A. M. Seifalian, *Biomedicines*, 2021, **10**(1), 73.
22 W. Guo, S. Wang, X. Yu, J. Qiu, J. Li, W. Tang, Z. Li, X. Mou, H. Liu and Z. Wang, *Nanoscale*, 2016, **8**, 1897–1904.
23 F. Emadi, A. Amini, A. Gholami and Y. Ghasemi, *Sci. Rep.*, 2017, **7**, 42258.
24 A. Rhazouani, H. Gamrani, M. El Achaby, K. Aziz, L. Gebrati, M. S. Uddin and F. Aziz, *BioMed Res. Int.*, 2021, **2021**, 5518999.
25 Z. Guo, P. Zhang, A. J. Chetwynd, H. Q. Xie, E. Valsami-Jones, B. Zhao and I. Lynch, *Nanoscale*, 2020, **12**, 18600–18605.
26 E. C. Qin, M. E. Kandel, E. Liamas, T. B. Shah, C. Kim, C. D. Kaufman, Z. J. Zhang, G. Popescu, M. U. Gillette, D. E. Leckband and H. Kong, *Acta Biomater.*, 2019, **90**, 412–423.
27 M. Lv, Y. Zhang, L. Liang, M. Wei, W. Hu, X. Li and Q. Huang, *Nanoscale*, 2012, **4**, 3861–3866.
28 P. Li, T. Xu, S. Wu, L. Lei and D. He, *J. Appl. Toxicol.*, 2017, **37**, 1140–1150.
29 M. Bramini, A. Rocchi, F. Benfenati and F. Cesca, *Adv. Neurobiol.*, 2019, **22**, 51–79.
30 M. Bramini, S. Sacchetti, A. Armirotti, A. Rocchi, E. Vazquez, V. Leon Castellanos, T. Bandiera, F. Cesca and F. Benfenati, *ACS Nano*, 2016, **10**, 7154–7171.

Open Access Article. Published on 09 Sunguti 2024. Downloaded on 2025-08-13 04:12:18.
This article is licensed under a Creative Commons Attribution-NonCommercial 3.0 Unported Licence.

31 M. Bramini, M. Chiacchiaretta, A. Armirotti, A. Rocchi, D. D. Kale, C. Martin, E. Vazquez, T. Bandiera, S. Ferroni, F. Cesca and F. Benfenati, *Small*, 2019, **15**, e1900147.
32 M. M. Ghazimoradi, F. Vahdatazad, F. Jalali and M. Rafieian-Kopaei, *Curr. Pharm. Des.*, 2022, **28**(44), 3572–3581.
33 K. Lawkowska, M. Pokrywczynska, K. Koper, L. A. Kluth, T. Drewa and J. Adamowicz, *Int. J. Mol. Sci.*, 2021, **23**(1), 33.
34 G. Audira, J. S. Lee, P. Siregar, N. Malhotra, M. J. M. Rolden, J. C. Huang, K. H. Chen, H. S. Hsu, Y. Hsu, T. R. Ger and C. D. Hsiao, *Environ. Pollut.*, 2021, **278**, 116907.
35 E. G. Afshar, A. Zarrabi, A. Dehshahri, M. Ashrafizadeh, G. Dehghannoudeh, B. Behnam, A. Mandegary, A. Pardakhty, R. Mohammadinejad and S. Tavakol, *FlatChem*, 2020, **22**, 100173.
36 O. Akhavan, E. Ghaderi, E. Abouei, S. Hatamie and E. Ghasemi, *Carbon*, 2014, **66**, 395–406.
37 M. Catanesi, G. Panella, E. Benedetti, G. Fioravanti, F. Perrozzi, L. Ottaviano, L. D. Leandro, M. Ardini, F. Giansanti, M. d'Angelo, V. Castelli, F. Angelucci, R. Ippoliti and A. Cimini, *Nanomedicine*, 2018, **13**, 3091–3106.
38 A. Franceschi Biagioni, G. Cellot, E. Pati, N. Lozano, B. Ballesteros, R. Casani, N. C. Coimbra, K. Kostarelos and L. Ballerini, *Biomaterials*, 2021, **271**, 120749.
39 M. G. Tupone, G. Panella, M. d'Angelo, V. Castelli, G. Caioni, M. Catanesi, E. Benedetti and A. Cimini, *Int. J. Mol. Sci.*, 2021, **22**(23), 13047.
40 G. Cellot, L. Jacquemin, G. Reina, A. Franceschi Biagioni, M. Fontanini, O. Chaloin, Y. Nishina, A. Bianco and L. Ballerini, *ACS Appl. Nano Mater.*, 2023, **6**, 8105.
41 A. H. Palejwala, J. S. Fridley, J. A. Mata, E. L. Samuel, T. G. Luerssen, L. Perlaky, T. A. Kent, J. M. Tour and A. Jea, *Surg. Neurol. Int.*, 2016, **7**, 75.
42 T. A. Tabish, M. Z. I. Pranjol, H. Hayat, A. A. M. Rahat, T. M. Abdullah, J. L. Whatmore and S. Zhang, *Nanotechnology*, 2017, **28**, 504001.
43 Q. R. Zhang, X. L. Liu, H. Y. Meng, S. J. Liu and C. D. Zhang, *Environ. Sci.: Nano*, 2018, **5**, 1361–1371.
44 V. Castagnola, L. Deleye, A. Podesta, E. Jaho, F. Loiacono, D. Debellis, M. Trevisani, D. Z. Ciobanu, A. Armirotti, F. Pisani, E. Flahaut, E. Vazquez, M. Bramini, F. Cesca and F. Benfenati, *Nano Lett.*, 2023, **23**, 2981–2990.
45 A. A. John, A. P. Subramanian, M. V. Vellayappan, A. Balaji, H. Mohandas and S. K. Jaganathan, *Int. J. Nanomed.*, 2015, **10**, 4267–4277.
46 R. Rauti, N. Lozano, V. Leon, D. Scaini, M. Musto, I. Rago, F. P. Ulloa Severino, A. Fabbro, L. Casalis, E. Vazquez, K. Kostarelos, M. Prato and L. Ballerini, *ACS Nano*, 2016, **10**, 4459–4471.
47 Q. Liu, G. Liu, X. Liu, M. Yang, S. Xing, Y. Du and X. Xiong, *Appl. Nanosci.*, 2020, **10**, 687–694.
48 J. Wang, Y. Cheng, L. Chen, T. Zhu, K. Ye, C. Jia, H. Wang, M. Zhu, C. Fan and X. Mo, *Acta Biomater.*, 2019, **84**, 98–113.
49 C. Dong, F. Qiao, W. Hou, L. Yang and Y. Lv, *Appl. Mater. Today*, 2020, **21**, 100870.
50 Z. Huang, Z. Guo, M. Sun, S. Fang and H. Li, *RSC Adv.*, 2019, **9**, 28627–28635.
51 D. Convertino, S. Luin, L. Marchetti and C. Coletti, *Front. Neurosci.*, 2018, **12**, 1.
52 D. Convertino, F. Fabbri, N. Mishra, M. Mainardi, V. Cappello, G. Testa, S. Capsoni, L. Albertazzi, S. Luin, L. Marchetti and C. Coletti, *Nano Lett.*, 2020, **20**, 3633–3641.
53 T. Song, K. Gu, W. Wang, H. Wang, Y. Yang, L. Yang, P. Ma, X. Ma, J. Zhao, R. Yan, J. Guan, C. Wang, Y. Qi and J. Ya, *J. Pharm. Sci.*, 2015, **104**, 3851–3860.
54 Z. Zhang, X. Wang, P. Li, M. Bai and W. Qi, *J. Biomater. Sci., Polym. Ed.*, 2021, **32**, 874–885.
55 M. Hanani, *Brain Res. Rev.*, 2005, **48**, 457–476.
56 R. S. Nascimento, M. F. Santiago, S. A. Marques, S. Allodi and A. M. Martinez, *Braz. J. Med. Biol. Res.*, 2008, **41**, 1011–1017.
57 H. Liu, L. Zhao, W. Gu, Q. Liu, Z. Gao, X. Zhu, Z. Wu, H. He, F. Huang and W. Fan, *J. Mol. Histol.*, 2018, **49**, 257–263.
58 C. Braccia, V. Castagnola, E. Vazquez, V. J. Gonzalez, F. Loiacono, F. Benfenati and A. Armirotti, *Carbon*, 2021, **185**, 591–598.
59 F. Alnasser, V. Castagnola, L. Boselli, M. Esquivel-Gaon, E. Efeoglu, J. McIntyre, H. J. Byrne and K. A. Dawson, *Nano Lett.*, 2019, **19**, 1260–1268.
60 M. Esquivel-Gaon, N. H. Nguyen, M. F. Sgroi, D. Pullini, F. Gili, D. Mangherini, A. I. Pruna, P. Rosicka, A. Sevcu and V. Castagnola, *Nanoscale*, 2018, **10**, 6539–6548.
61 M. Kucki, L. Diener, N. Bohmer, C. Hirsch, H. F. Krug, V. Palermo and P. Wick, *J. Nanobiotechnol.*, 2017, **15**, 46.
62 H. Suzuki, T. Toyooka and Y. Ibuki, *Environ. Sci. Technol.*, 2007, **41**, 3018–3024.
63 S. Thongrattanasiri, F. H. Koppens and F. J. Garcia de Abajo, *Phys. Rev. Lett.*, 2012, **108**, 047401.
64 O. Benzina, V. Szabo, O. Lucas, M. B. Saab, T. Cloitre, F. Scamps, C. Gergely and M. Martin, *J. Biomed. Opt.*, 2013, **18**, 106014.
65 M. Martin, O. Benzina, V. Szabo, A. G. Vegh, O. Lucas, T. Cloitre, F. Scamps and C. Gergely, *PLoS One*, 2013, **8**, e56286.
66 P. Valente, G. Lignani, L. Medrihan, F. Bosco, A. Contestabile, P. Lippiello, E. Ferrea, M. Schachner, F. Benfenati, S. Giovedi and P. Baldelli, *J. Cell Sci.*, 2016, **129**, 1878–1891.
67 C. Prestigio, D. Ferrante, P. Valente, S. Casagrande, E. Albanesi, Y. Yanagawa, F. Benfenati and P. Baldelli, *Mol. Neurobiol.*, 2019, **56**, 6276–6292.
68 S. A. Scott, *Sensory Neurons: Diversity, Development, and Plasticity*, Oxford University Press, 1992.
69 R. Waldmann, G. Champigny, E. Lingueglia, J. R. De Weille, C. Heurteaux and M. Lazdunski, *Ann. N. Y. Acad. Sci.*, 1999, **868**, 67–76.
70 M. Petersen and R. H. LaMotte, *Pain*, 1993, **54**, 37–42.

This journal is © The Royal Society of Chemistry 2024

Open Access Article. Published on 09 Sunguti 2024. Downloaded on 2025-08-13 04:12:18.
This article is licensed under a Creative Commons Attribution-NonCommercial 3.0 Unported Licence.

71 P. Holzer, *Handb. Exp. Pharmacol.*, 2009, **194**, 283–332.
72 L. A. Pattison, G. Callejo and E. St John Smith, *Philos. Trans. R. Soc. London, Ser. B*, 2019, **374**, 20190291.
73 T. Yamada, S. Ugawa, T. Ueda, Y. Ishida, K. Kajita and S. Shimada, *J. Histochem. Cytochem.*, 2009, **57**, 277–287.
74 N. Alessandri-Haber, J. J. Yeh, A. E. Boyd, C. A. Parada, X. Chen, D. B. Reichling and J. D. Levine, *Neuron*, 2003, **39**, 497–511.
75 F. Fujita, K. Uchida, Y. Takayama, Y. Suzuki, M. Takaishi and M. Tominaga, *J. Physiol. Sci.*, 2018, **68**, 431–440.
76 A. Gomis, S. Soriano, C. Belmonte and F. Viana, *J. Physiol.*, 2008, **586**, 5633–5649.
77 T. Quallo, N. Vastani, E. Horridge, C. Gentry, A. Parra, S. Moss, F. Viana, C. Belmonte, D. A. Andersson and S. Bevan, *Nat. Commun.*, 2015, **6**, 7150.
78 G. Callejo, J. P. Giblin and X. Gasull, *PLoS One*, 2013, **8**, e64471.
79 B. Flores and E. Delpire, *Cell. Physiol. Biochem.*, 2020, **54**, 577.
80 C. Montell, *Sci. STKE*, 2005, (272), re3.
81 N. Damann, T. Voets and B. Nilius, *Curr. Biol.*, 2008, **18**, R880–R889.
82 M. J. Caterina, M. A. Schumacher, M. Tominaga, T. A. Rosen, J. D. Levine and D. Julius, *Nature*, 1997, **389**, 816–824.
83 M. Tominaga and T. Tominaga, *Pflugers Arch.*, 2005, **451**, 143–150.
84 P. Valente, A. Fernandez-Carvajal, M. Camprubi-Robles, A. Gomis, S. Quirce, F. Viana, G. Fernandez-Ballester, J. M. Gonzalez-Ros, C. Belmonte, R. Planells-Cases and A. Ferrer-Montiel, *FASEB J.*, 2011, **25**, 1628–1640.
85 G. M. Story, A. M. Peier, A. J. Reeve, S. R. Eid, J. Mosbacher, T. R. Hricik, T. J. Earley, A. C. Hergarden, D. A. Andersson, S. W. Hwang, P. McIntyre, T. Jegla, S. Bevan and A. Patapoutian, *Cell*, 2003, **112**, 819–829.
86 K. Nagata, A. Duggan, G. Kumar and J. Garcia-Anoveros, *J. Neurosci.*, 2005, **25**, 4052–4061.
87 M. J. Caterina, A. Leffler, A. B. Malmberg, W. Martin, J. Trafton, K. Petersen-Zeitz, M. Koltzenburg, A. Basbaum and D. Julius, *science*, 2000, **288**, 306–313.
88 N. Liessi, L. Maragliano, V. Castagnola, M. Bramini, F. Benfenati and A. Armirotti, *Anal. Chem.*, 2021, **93**, 784–791.
89 D. E. Owen, *Methods in Molecular Biology, in Neurotrophic Factors*, 2012, **846**(16), 179–187.
90 M. Richner, S. B. Jager, P. Siupka and C. B. Vaegter, *J. Visualized Exp.*, 2017, **22**(119), 55226.
91 R. Bruderer, O. M. Bernhardt, T. Gandhi, S. M. Miladinović, L.-Y. Cheng, S. Messner, T. Ehrenberger, V. Zanotelli, Y. Butscheid and C. Escher, *Mol. Cell. Proteomics*, 2015, **14**, 1400–1410.
92 Z. Pang, G. Zhou, J. Ewald, L. Chang, O. Hacariz, N. Basu and J. Xia, *Nat. Protoc.*, 2022, **17**, 1735–1761.
93 D. Szklarczyk, A. L. Gable, D. Lyon, A. Junge, S. Wyder, J. Huerta-Cepas, M. Simonovic, N. T. Doncheva, J. H. Morris and P. Bork, *Nucleic Acids Res.*, 2019, **47**, D607–D613.
94 A. E. Carpenter, T. R. Jones, M. R. Lamprecht, C. Clarke, I. H. Kang, O. Friman, D. A. Guertin, J. H. Chang, R. A. Lindquist, J. Moffat, P. Golland and D. M. Sabatini, *Genome Biol.*, 2006, **7**, R100.
95 C. A. Warwick, A. L. Keyes, T. M. Woodruff and Y. M. Usachev, *J. Biol. Chem.*, 2021, **297**, 101085.